CHEMISTRY
AN ASIAN JOURNAL
ACES
FULL PAPER

DOI: 10.1002/asia.201402078

Construction and DNA Condensation of Cyclodextrin-Coated Gold Nanoparticles with Anthryl Grafts

Di Zhao, Yong Chen, and Yu Liu*[a]

Abstract: The condensation of DNA in a controlled manner is one of the key steps in gene delivery and gene therapy. For this purpose, a water-soluble supramolecular nanostructure is constructed by coating 14 β-cyclodextrins onto the surface of a gold nanoparticle, followed by the noncovalent association of different amounts of anthryl-modified adamantanes with coated β-cyclodextrins. The strong binding of β-cyclodextrins with anthryl adamantanes ($K_S = 8.61 \times 10^4\ M^{-1}$) efficiently stabilizes the supramolecular nanostructure. Spectrophotometric fluorescence spectra and microscopic studies demonstrated that, with many anthryl grafts that can intercalate in the outer space of the DNA double helix, this supramolecular nanostructure showed good condensation abilities to calf thymus DNA. Significantly, the condensation efficiency of supramolecular nanostructure towards DNA could be conveniently controlled by adjusting the ratio between gold nanoparticles and anthryl adamantane grafts, leading to the formation of DNA condensates of a size that are suitable for the endocytosis of hepatoma cells, which will make it potentially applicable in many fields of medicinal science and biotechnology.

Keywords: cyclodextrins · cytotoxicity · DNA · gene technology · host–guest systems

Introduction

Gene therapy is the use of genes (DNA and RNA) instead of conventional drugs to treat diseases. After the first successful case of gene therapy occurred in 1990,[1] significant progress has been made in this area over past two decades. Considering that naked genes are not effectively endocytosed by cells and are easily degraded by serum nucleases,[2] it is important for scientists to find efficient and safe gene-delivery systems.[3] Nowadays, several kinds of functional systems, such as viruses,[4] lipoplexes,[5] polyplexes,[6] dendrimers,[7] and inorganic metal nanoparticles,[8] have been widely used as vectors for gene therapy. Among them, gold nanoparticles (AuNPs) have attracted increasing attention because of their unique chemical and physical properties, such as high surface-to-volume ratios, being essentially inert, nontoxicity,[9] ease of preparation, high transfection efficiency, and high drug transportation ability.[10] Rotello et al. reported that tetraalkylammonium ligand modified AuNPs could interact with the DNA backbone through charge complementarity.[11] They also developed light-triggered DNA release by AuNP, which was modified with a quaternary ammonium salt, through a photocleavable *o*-nitrobenzyl ester linker.[12] Klibanov and Thomas demonstrated that AuNPs functionalized with branched polyethylenimine (PEI) chains were 12 times more efficient than unmodified PEI.[13] Although AuNP-based gene-delivery systems have been investigated extensively, most of these systems involve the covalent linkage of functional molecules to the AuNP surface. As a result, the preparation processes for these kinds of vectors are usually complex and it becomes difficult to adjust the DNA condensing capabilities of vectors without changing the ratio of the reactants when preparing AuNPs.

Supramolecular chemistry, which is the chemistry of noncovalent interactions, provides an easy way to construct complicated and controllable molecular assemblies for applications in biomedical science. A number of host–guest supramolecular systems have been reported for gene and drug delivery.[14] Of all macrocyclic host molecules, cyclodextrins (CDs), which are cyclic oligosaccharides composed of six to eight D-glucopyranoside units, have attracted great interest for their benign water solubility, low toxicity, biological compatibility, and unique inclusion ability for various organic or biological molecules that fit their hydrophobic cavity. Therefore, CDs are extensively applied in biochemistry and pharmaceuticals, such as enhancing cell membrane absorption,[15] increasing the nuclease resistance of oligonucleotides,[16] reducing the immunostimulatory response,[17] and compacting and carrying DNA into cells.[8, 18] In preliminary research, we found that oligo(ethylenediamine)-β-CD-modified AuNP can concentrate and carry DNA into cells.[8] We also found that β-CD based supramolecular architectures with aryl grafts could act as promising DNA concentrators.[8, 18] These findings led us to the design and construction of supramolecular architectures based on CDs and

[a] D. Zhao, Dr. Y. Chen, Prof. Dr. Y. Liu
Department of Chemistry
State Key Laboratory of Elemento-Organic Chemistry
Collaborative Innovation Center of Chemical
Science and Engineering (Tianjin)
Nankai University, Tianjin, 300071 (P.R. China)
E-mail: yuliu@nankai.edu.cn

Supporting information for this article is available on the WWW under http://dx.doi.org/10.1002/asia.201402078.

AuNPs, and one could hypothesize that the combination of CDs and AuNPs, especially nanometer-scaled CD-AuNP systems, might lead to a breakthrough in many fields of chemistry and materials science. Herein, we report a soluble nanometer-scaled AuNPs system noncovalently grafted by anthryl groups (Scheme 1). Considering the controllable association between the CD-modified AuNP core (**2**) and anthryl grafts through host–guest binding of the β-CD cavity with anthryl adamantine (**3**), the DNA condensation capabilities of the desired nanostructure can be conveniently tuned by adjusting the **2**/**3** ratio.

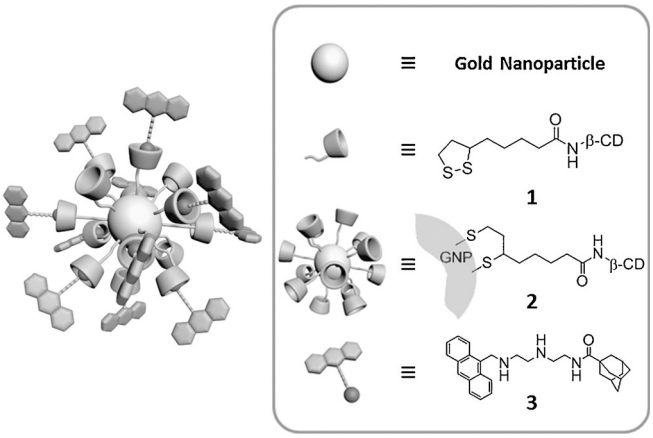

Scheme 1. Construction of the CD-AuNP (**2**)/anthryl adamantine (**3**) host–guest system.

Results and Discussion

Characterization of 2

β-CD-coated AuNPs were obtained by the reaction of **1** with gold chloride tetrahydrate and were characterized by ^{1}H and ^{13}C NMR spectroscopy, elemental analysis, and inductively coupled plasma atomic emission spectroscopy (ICP-AES). FTIR spectra showed that the shape of the FTIR spectrum of β-CD-coated AuNPs (**2**) was similar to that of free **1**, accompanied by the clear broadening of several characteristic peaks (Figure S1 in the Supporting Information).

In addition, thermogravimetric analysis (TGA) showed that **1** rapidly decomposed at approximately 330 °C, accompanied by 68.5 % weight loss up to 800 °C (Figure 1); however, **2** presented a smooth and slow weight loss and only gave 14.5 % weight loss up to 800 °C. Through a calculation based on the weight losses of **1** and **2** within 800 °C, the content of units of **1** in **2** was measured to be 21.2 %, which corresponded to a W_{CD} value of 0.159 mmol g^{-1}. This result is in accordance with the result calculated from elemental analysis and ICP-AES data (W_{CD} = 0.162 mmol g^{-1}; Table 1)

Table 1 shows the elemental analysis of **2**. By assuming that the core shape of the nanoparticles is spherical, the

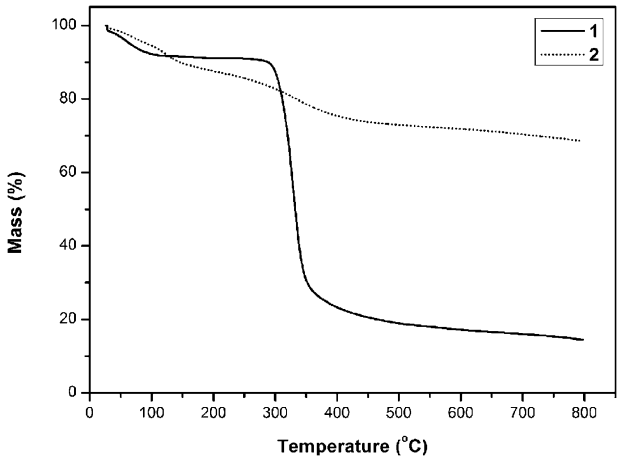

Figure 1. TGA results for **1** and **2**.

Table 1. Elemental analysis of **2**.

Element	Analysis method	Content [%]
Au	ICP-AES	25.7
C	Vario EL Cube[a]	9.73
H	Vario EL Cube[a]	2.73
N	Vario EL Cube[a]	0.30

[a] See the Experimental Section for more details about the Vario EL Cube analyzer.

average number of gold atoms per AuNP and the average number of CD units around one nanoparticle (N_{CD}) could be calculated by means of Equations (1)–(4).[19]

$$U = \frac{2}{3}\pi\left(\frac{D}{a}\right)^3 \quad (1)$$

$$W_{NP} = \frac{M_{Au}}{m_{Au}U} \quad (2)$$

$$W_{CD} = \frac{M_C}{m_{CD}n} \quad (3)$$

$$N_{CD} = \frac{W_{CD}}{W_{NP}} = \frac{M_C m_{Au} U}{m_{CD} M_{Au} n} \quad (4)$$

in which U is the number of gold atoms per AuNP; D is the average diameter of AuNPs; a refers to the edge of a gold unit cell, which has a value of 4.0786 Å; M_{Au} and M_C are the gold and carbon contents, respectively; m_{Au} and m_{CD} are the atomic weight of gold and the molecular weight of host **1**, respectively; W_{NP} and W_{CD} are contents of AuNPs and host **1**, respectively; and n is the number of carbon atoms per host **1**. The results of the calculations are as follows: U = 1109, $W_{NP} = 1.18\times10^{-6}$ mol g^{-1}, $W_{CD} = 1.62\times10^{-4}$ mol g^{-1}, and N_{CD} = 14.

Binding of the β-CD Cavity with 3

To investigate quantitatively the inclusion complexation behavior of the β-CD cavity with **3** and their thermodynamic origins, isothermal titration calorimetry (ITC) experiments were performed in water. The VP-ITC instrument was calibrated chemically by measurement of the complexation reaction of β-CD with cyclohexanol, and the obtained thermodynamic data were shown to be in good agreement (error < 2%) with the literature data.[20] All microcalorimetric titrations between β-CD and **3** were performed in aqueous solution at atmospheric pressure and 298.15 K to give the complex stability constants (K_S) and thermodynamic parameters. Twenty-five successive injections were made for each titration experiment. In each run, an aqueous solution of host in a 250 μL syringe was sequentially injected with stirring at 300 rpm into an aqueous solution of guest in the sample cell (1.4227 mL volume). Figure 2 shows a representative titration curve; each titration of β-CD into the sample cell gave an apparent reaction heat caused by the formation of an inclusion complex between β-CD and **3**. A control experiment to determine the heat of dilution was performed for each run by performing the same number of injections with the same concentration of host compound as that used in the titration experiments into water. The net reaction heat was given by subtracting the dilution heat from the apparent reaction heat.

Generally, the first point of the titration curve was disregarded because some liquid mixing near the tip of the injection needle was known to occur at the beginning of each ITC run. Two independent titration experiments were performed to afford self-consistent parameters and to give averaged values. The binding stoichiometry (N), complex stability constant (K_S), standard molar reaction enthalpy (ΔH^o), and standard deviation were obtained by using the "one set of binding sites" model (Origin software, Microcal Inc.). The standard free energy (ΔG^o) and entropy changes (ΔS^o) were calculated according to Equation (5)

$$\Delta G^o = -RT\ln K_S = \Delta H^o - T\Delta S^o \quad (5)$$

in which R is the gas constant and T is the absolute temperature. Figure 3 shows a typical curve fitting result for the complexation of **3** with β-CD in water. From the ITC results, complex stability constants (K_S), enthalpic changes (ΔH^o), and entropic changes ($T\Delta S^o$) for the complexation of β-CD and **3** were determined to be $[(8.61\pm0.05)\times10^4]\,M^{-1}$, $(-31.99\pm0.36)\,kJ\,mol^{-1}$, and $(-3.85\pm0.37)\,kJ\,mol^{-1}$, respectively.

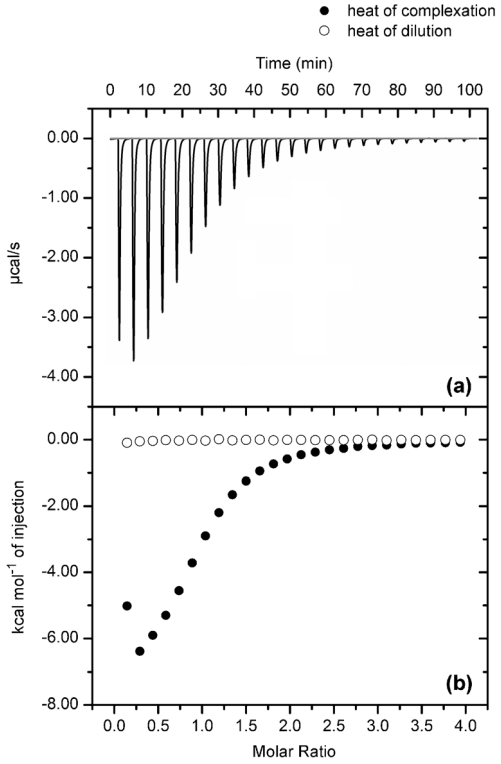

Figure 2. Microcalorimetric titration of **3** with β-CD in aqueous solution at 298.15 K. a) Raw ITC data for 25 sequential injections (10 μL per injection) of a solution of β-CD (2.02 mM) into a solution of **3** (0.097 mM). b) Heat effects of the dilution and complexation reaction of **3** with β-CD for each injection during the microcalorimetric titration experiment.

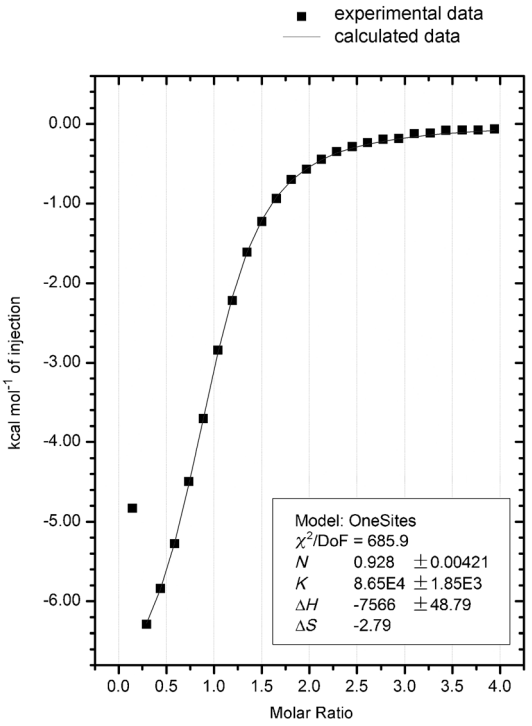

Figure 3. "Net" heat effects of complexation of β-CD with **3** for each injection, obtained by subtracting the dilution heat from the reaction heat, which was fitted by computer simulation with the "one set of binding sites" model.

2D ROESY NMR Spectroscopy

2D NMR spectroscopy has become a powerful method to study the conformations of host–guest complexes. NOE correlation signals in the NOESY or ROESY spectrum means that two protons are closely located in space (0.4 nm apart at most).[21] The inclusion structure of **3** and β-CD was identified by 2D ROESY spectroscopy (Figure 4). It is known

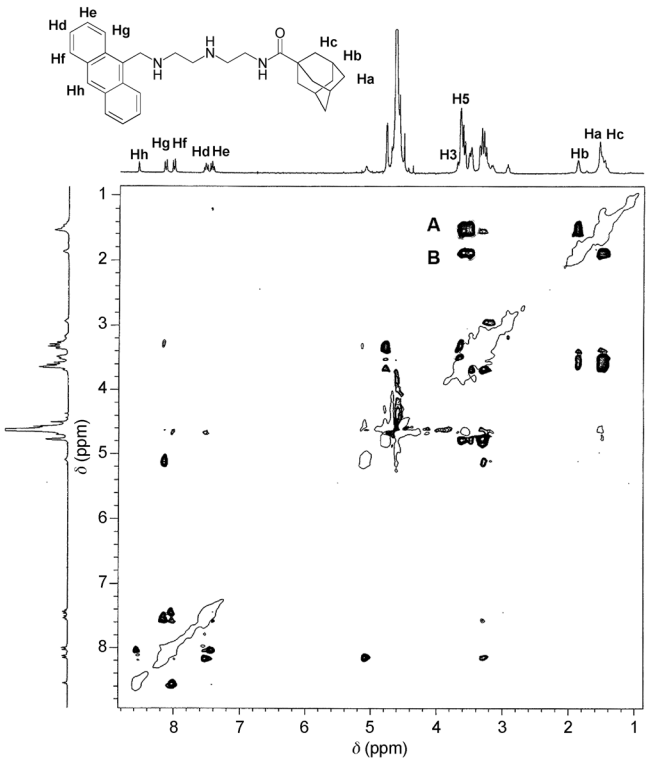

Figure 4. The 2D ROESY spectrum of **3** and β-CD in D_2O with a mixing time of 250 ms.

that only the H3, H5, and H6 protons of CDs can give the NOE cross-peaks for analyzing the conformation of host–guest complexes because the H2 and H4 protons face the outer cavity. As shown in Figure 4, all 15 protons of the adamantane group present clear cross-peaks with the H3 and H5 protons. Moreover, no NOE correlation signal was detected between the protons of the anthryl group and β-CD. These results unambiguously showed that the adamantane group of **3** was included in the β-CD cavity through the wide opening and the anthyl group was located out of the β-CD cavity and had a chance to react with the DNA backbone.

DNA Binding Behavior of 3

The DNA binding behavior of **3** was investigated by the fluorescence titrations, in which calf thymus DNA (ct-DNA) of different concentrations was gradually added to a solution of β-CD/**3** complex, and the fluorescence emissions were recorded (Figure 5). The β-CD was used as a competitive reagent to exclude probable interactions between the adamantane group and ct-DNA. Binding of the anthryl group to the

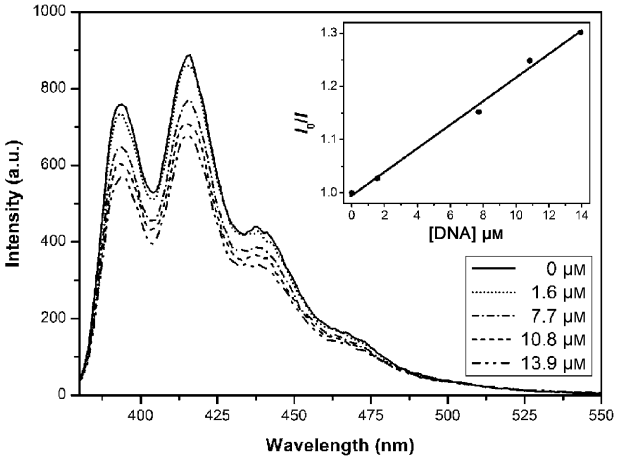

Figure 5. The fluorescence intensity of β-CD/**3** (0.10 mM/0.01 mM) with increasing concentrations of ct-DNA (0–13.9 μM) in 5 mM Tris-HCl and 50 mM NaCl buffer (pH 7.1), with excitation at $\lambda = 366$ nm. Inset: Stern–Volmer quenching plot of **3** with increasing concentrations of ct-DNA, with excitation at $\lambda = 366$ nm and monitored at $\lambda = 415$ nm.

DNA helix quenched the fluorescence very strongly. The fluorescence quenching data were plotted according to Equation (6),[22] in which I_o and I are the fluorescence intensities in the absence and presence of DNA, respectively; and K_{SV} is the Stern–Volmer quenching constant, which is a measure of the efficiency of quenching by DNA.

$$I_o/I = 1 + K_{SV}[\mathrm{DNA}] \quad (6)$$

As shown in Figure 5, the fluorescence intensity of **3** decreased gradually with increasing concentration of ct-DNA. The fluorescence quenching constant evaluated by using Equation (6) was $2.2 \times 10^4\ \mathrm{M}^{-1}$ of DNA phosphates.

The DNA binding behavior of **3** was also investigated by ^{1}H NMR spectroscopy. As shown in Figure 7b below, the signals of anthryl protons gradually broadened, accompanied by slight chemical shift changes with the addition of ct-DNA. This phenomenon also demonstrated the intercalation of the anthryl groups into the hydrophobic DNA double helix.

Absorption Spectra

To investigate the aggregation behavior of **2**/**3** with DNA, the absorption spectra of **2** and **2**/**3** were recorded in the absence and presence of ct-DNA at varying concentrations. Because the absorption band of **2** at $\lambda = 260$ nm overlapped with that of ct-DNA, we only analyzed the absorption maximum of **2** beyond $\lambda = 450$ nm, which was assigned to the surface plasmon resonance (SPR) band of AuNP. Generally, because of electric dipole–dipole interactions and coupling

between the neighboring particles in the aggregates of gold particles, the SPR band of gold particles will show an appreciate bathochromic shift in the UV absorption spectrum.[23] As shown in Figure 6a, the addition of ct-DNA to an aqueous solution of the **2**/**3** system produced a bathochromic shift of the SPR maximum from $\lambda = 508$ to 519 nm, accompanied by the increased intensity of the SPR band. This phenomenon indicated an effective aggregation of AuNPs. For comparative purposes, the absorption spectra of **2** in the presence of ct-DNA at varying concentrations were also recorded (Figure S8 in the Supporting Information). The UV absorption band of **2** was almost unchanged upon the gradual addition of DNA. This phenomenon means that there is no appreciable aggregation of **2** without **3**. In addition, the absorption changes of **2** in the presence of a constant concentration of ct-DNA and different concentrations of **3** were also recorded (Figure 6b) to compare the effect of the surface coverage of **3** on the interactions of **2**/**3** with DNA. As shown in Figure 6b, the addition of **3** to an aqueous solution of **2**+ct-DNA also led to a bathochromic shift (7 nm) and increased intensity of the SPR band; this indicated that the increased surface coverage of **3** promoted the reactivity of **2**/**3** with DNA.

^{1}H NMR Spectroscopy

The aggregation behavior of **2**/**3** with DNA was also investigated by ^{1}H NMR spectroscopy. Figure 7a shows the partial ^{1}H NMR spectra of **2** (5.0×10^{-4} M) and a mixture of **2** (5.0×10^{-4} M) and ct-DNA (1.0×10^{-3} M) in D_2O by adding 0, 5.0×10^{-5}, 1.0×10^{-4}, 2.0×10^{-4}, 2.5×10^{-4}, or 5.0×10^{-4} M of **3**. The signals of **2** gradually broadened and shift upfield with the increasing guest/host ratio in the presence of ct-DNA. This phenomenon may indicate the formation of tight supramolecular complexes between DNA and **2**/**3**,[8,18] and the condensation efficiency of **2**/**3** could be controlled by changing the guest/host ratio.

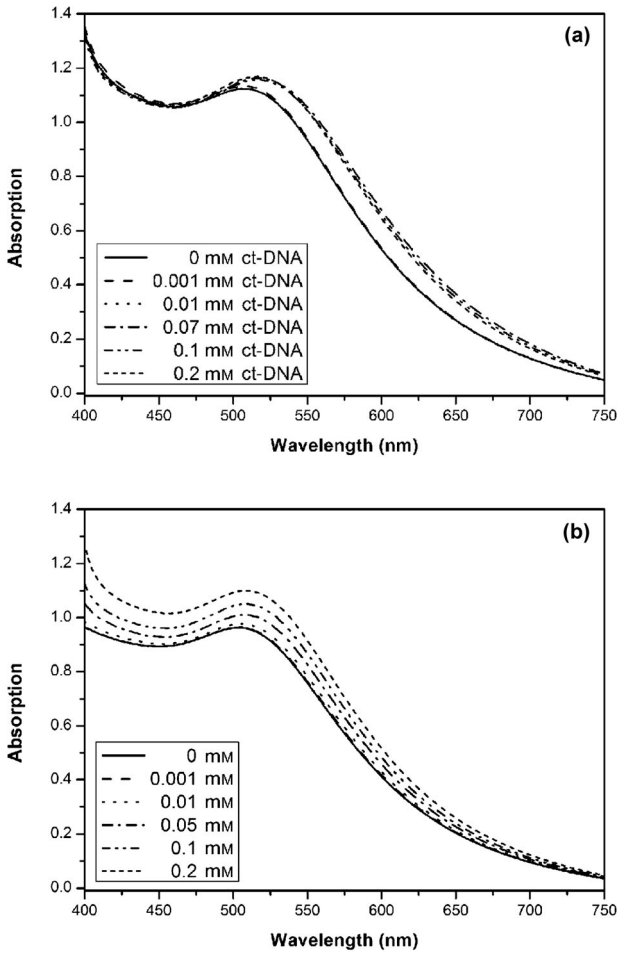

Figure 6. a) UV/Vis absorption spectra of **2**/**3** (0.62 g L^{-1}/0.2 mM) in the presence of ct-DNA at different concentrations in water (pH 7.0). b) UV/Vis absorption spectra of **2**/ct-DNA (0.62 g L^{-1}/0.18 g L^{-1}) in the presence of **3** at different concentrations in water (pH 7.0).

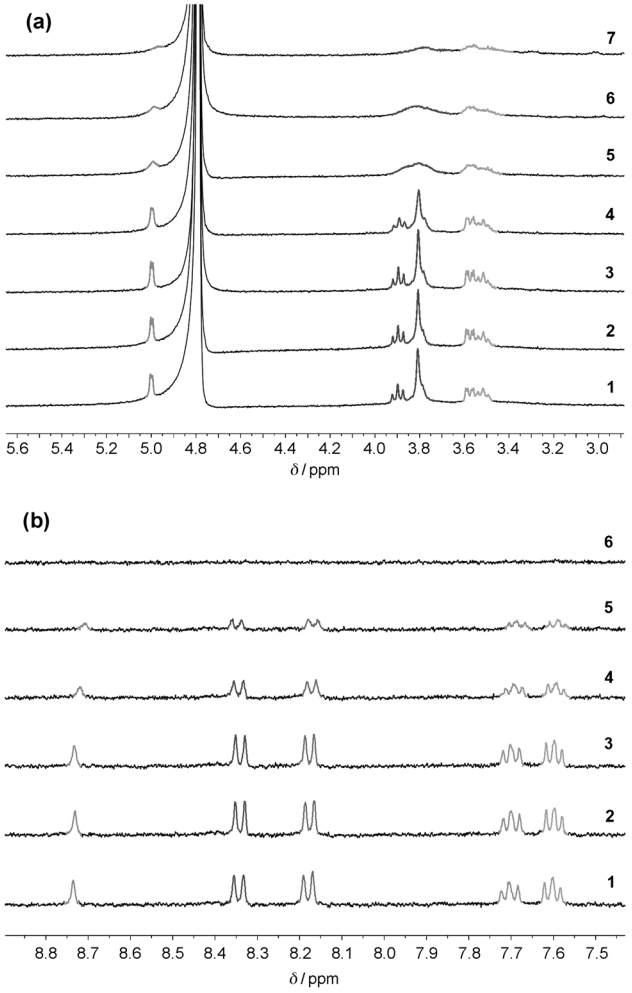

Figure 7. a) Partial ^{1}H NMR spectra of **2** (1; 5.0×10^{-4} M) and the mixture of **2** (5.0×10^{-4} M) and ct-DNA (1.0×10^{-3} M) in D_2O by adding 0, 5.0×10^{-5}, 1.0×10^{-4}, 2.0×10^{-4}, 2.5×10^{-4}, or 5.0×10^{-4} M of **3** (2 to 7). b) Partial ^{1}H NMR spectra of **3** (5.0×10^{-4} M) in D_2O by adding 0, 5.0×10^{-5}, 1.0×10^{-4}, 2.5×10^{-4}, 5.0×10^{-4}, or 1.0×10^{-3} M of ct-DNA (1 to 6).

Microscopy

Direct information about the size, shape, and distribution of **2/3** and its aggregates with DNA came from AFM and TEM results. Figure 8 shows typical AMF images of ct-DNA in the absence and presence of **2/3**. As shown in Figure 8a,

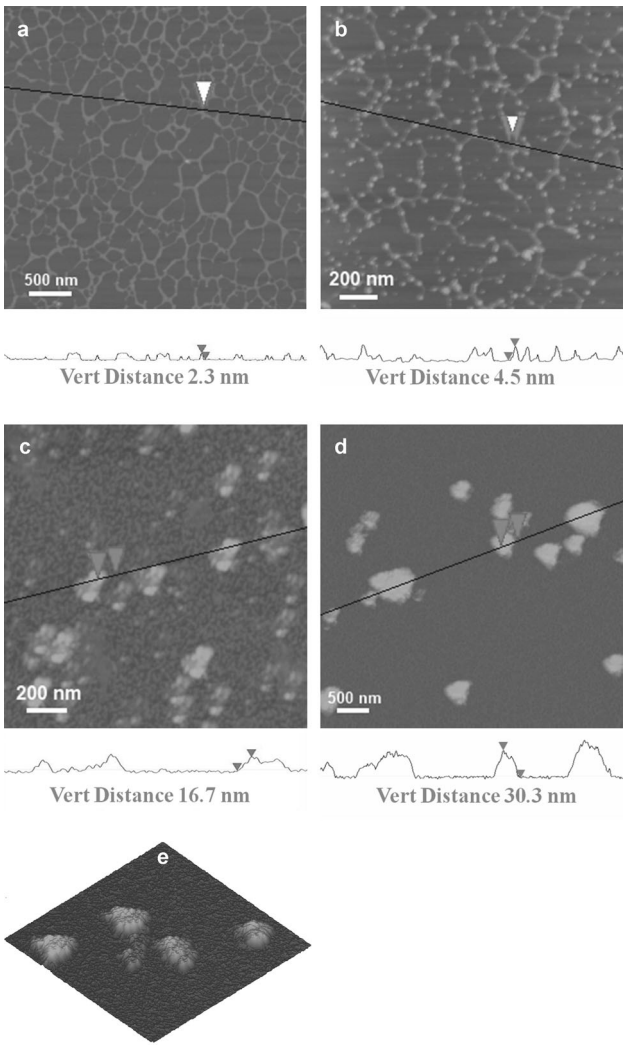

Figure 8. AFM images of ct-DNA (0.37 g L^{-1}) in the absence (a) and presence of **2/3** with different guest/host ratios (1:20 (b), 1:5 (c), and 1:1 (d)). e) Partial 3D view of d).

free ct-DNA was loose and silklike with a height of approximately 2.3 nm (typical diameter of DNA).[24] When **3** and **2** were added in different guest/host ratios (1:20, 1:5, and 1:1), host **2** tended to aggregate. As shown in Figure 8b, at a low guest/host ratio (1:20), most of the AuNPs still existed as discrete particles and some of them began to come into contact with DNA strands. When the guest/host ratio increased to 1:5, loose DNA strands could not be observed, and small aggregates formed with a height of approximately 16.7 nm (Figure 8c). When the guest/host ratio further increased to 1:1, discrete AuNPs tended to form large aggregates with a height of approximately 30.3 nm (Figure 8d). The 3D view of supramolecular aggregates clearly shows that the large aggregates are composed of smaller tight particles (Figure 8e). In contrast, the AMF images of **2** and **2/3** (Figure S9 in the Supporting Information) indicated that free **2** and **2/3** existed as dispersed solid particles with heights of approximately 3.5 and 4.1 nm, respectively. A similar phenomenon also was observed by TEM. Under our experimental conditions, host **2** existed as dispersed solid particles with an average core diameter of (3.3 ± 0.5) nm (based on individual measurements on at least 100 particles; Figure 9a). When

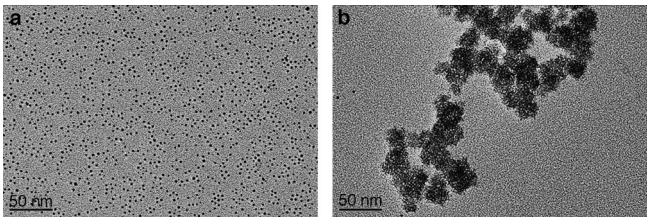

Figure 9. TEM images of a) **2** (0.62 g L^{-1}) and b) **2/3** (0.62 g L^{-1}, 0.10 mM) with DNA (0.37 g L^{-1}).

only **3** (Figure S10a in the Supporting Information) or ct-DNA (Figure S10b in the Supporting Information) were added individually, no appreciable aggregation of AuNPs was observed. Comparatively, when **3** and ct-DNA were added, host **2** tended to gather together and large aggregates of AuNPs with an average diameter of (33.3 ± 7.4) nm were observed (Figure 9b); this indicated that small tight particles tended to form larger fluffy structures. This phenomenon demonstrated that complexes of **2/3** could act as promising DNA concentrators and gave good binding abilities toward ct-DNA and the condensation efficiency could be conveniently controlled by adjusting the ratio between the AuNPs and anthryl adamantane grafts. From the viewpoint of biology, the larger size of the DNA condensates is favorable for their intracellular uptake and the smaller size of free **2/3** complexes means that the complexes can be eliminated faster from the cell after completing the delivery mission.[25] Specifically, DNA condensates of this size (~40 nm) could be preferentially internalized by the Hepa 1–6 hepatoma cell line through clathrin-mediated endocytosis.[26]

Zeta Potential

As shown in Table 2, the zeta potential of **2** slightly increased after being mixed with **3**, probably because the surface charge of nanoparticles was partly shielded by uncharged guest. The zeta potential of **2/3** decreased after being mixed with ct-DNA because the surface of the nanoparticles was covered by negatively charged DNA. Generally, electrostatic interactions are considered to be the main driving force for the condensation of DNA by complexation with condensing agents, such as multivalent cations,[27] peptides,[28] cationic polymers, and dendrimers.[29] On the other

Table 2. Zeta potential data for the nanoparticles.

Nanoparticle	Zeta potential [mV]
2[a]	−18.19
2/**3**[a]	−15.64
2[a] + ct-DNA[b]	−18.04
2/**3**[a] + ct-DNA[b]	−20.69

[a] [CD] = [**3**] = 0.10 mM. [b] [ct-DNA] = 0.05 mM.

hand, the intercalation of aryl grafts into DNA also contributes to the condensation of DNA in cooperation with cationic compounds.[8, 18] Considering the negative zeta potential of the **2**/**3** complex, intercalation should be the only driving force to condense DNA in the present system. The binding constant of aryl grafts with DNA is commonly in the order of $10^4\,M^{-1}$ in DNA base pairs.[22] Therefore, intercalation may be not very strong, which is consist with the results of microscopy that large aggregates formed by adjusting the guest/host ratio, but not very compact, and that very high nanoparticle and ct-DNA concentrations should be used for spectroscopy and microscopy studies.

Agarose Gel Electrophoresis

The formation of **2**/**3**/DNA complexes was analyzed by their electrophoretic mobility on an agarose gel at various w/w/w ratios. As shown in Figure 10a, the interaction of the **2**/**3** complex ([CD]/[**3**] = 1:1) with DNA is molar ratio dependent. As the concentration of **2**/**3** increased, the gel mobility of DNA decreased, and DNA was totally retained in the gel well at a $w_{CD\text{-}AuNP}/w_{\mathbf{3}}/w_{DNA}$ ratio of 43:3:1. Figure 10b shows the agarose gel assay of DNA in the presence of complex **2**/**3** at different guest/host ratios. The grafting of different amounts of **3** by **2** showed different condensation abilities and DNA was totally retained in the gel well at a guest/host molar ratio of 2:5; this means the condensation efficiency of **2**/**3** could be conveniently controlled by changing the guest/host ratio. In addition, the transfection experiments were also performed in HGC-27 human gastric carcinoma cells, which were tested with pCMV-AC-GFP DNA, and no visible green fluorescent protein (GFP) expression was observed. We think that improvements may be achieved by the further chemical modification of carriers, the appropriate selection of cells and DNA, and the optimization of the ratio of carriers and DNA in the mixture.

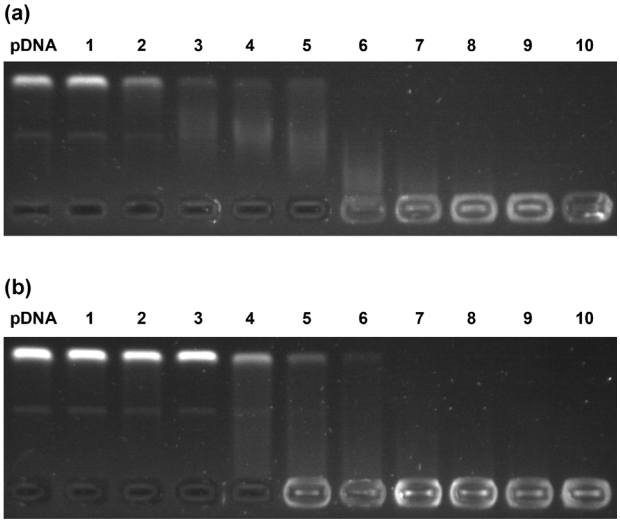

Figure 10. Agarose gel electrophoresis assay of pBR322 DNA (10 ng μL^{-1}). a) [CD] = 0, 0.01, 0.02, 0.03, 0.04, 0.05, 0.06, 0.07, 0.08, and 0.10 mM from lanes 1 to 10, respectively. [**3**] = 0.10, 0.01, 0.02, 0.03, 0.04, 0.05, 0.06, 0.07, 0.08, and 0.10 mM from lanes 1 to 10, respectively. b) [CD] = 0.10 mM from lanes 1 to 10. [**3**] = 0, 0.01, 0.02, 0.03, 0.04, 0.05, 0.06, 0.07, 0.08, and 0.10 mM from lanes 1 to 10, respectively.

Cytotoxicity Assay

Cytotoxicity assay results of aggregates of **2**/**3** with different concentrations are presented in Figure 11. We can see that aggregates of **2**/**3** exhibit no measurable cytotoxicity up to a concentration of 1 mM. The low cytotoxicity of aggregates of **2**/**3** probably arose from extrusive CD cavities on the surface of aggregates of **2**/**3** protecting the plasma membranes of cells from deposition by gold clusters.[8] The low cytotoxicity can also be attributed to its negative zeta potential (Table 2).

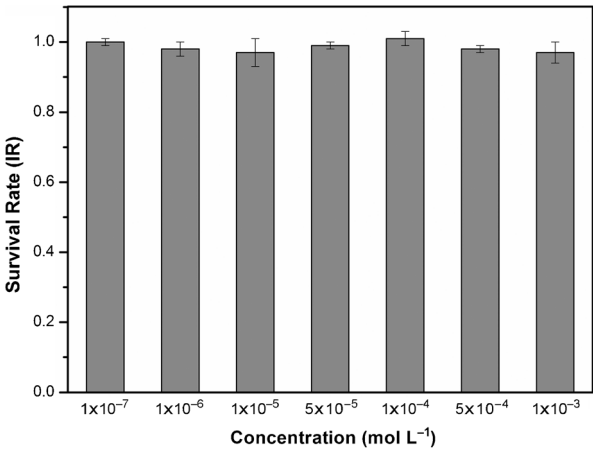

Figure 11. Cytotoxicity assay results for aggregates of **2**/**3** with different concentrations.

Conclusion

We constructed a water-soluble, nontoxic, nanometer-sized conjugate containing AuNPs, β-CDs, and anthryl adamantanes through a supramolecular assembly approach. Owing to the good DNA reactivity of anthracene moieties, this supramolecular conjugate exhibited good condensation abilities toward ct-DNA, and the condensation efficiency could be conveniently controlled through the binding equilibrium of CD cavities attached to the surfaces of AuNPs with anthryl adamantine grafts. The larger size of the DNA supramolecular aggregates was beneficial to their intracellular uptake and the smaller size of free complexes of **2**/**3** meant

the complexes could be eliminated faster from the cell after completion of the delivery mission. Owing to these findings, this supramolecular nanostructure is expected to have exciting applications in gene therapy with the promising potential to control gene expression and delivery.

Experimental Section

Materials

All solvents and reagents were commercially available and used without further purification, unless otherwise noted. Anhydrous *N*,*N*-dimethylformamide (DMF) was dried and distilled over CaH_2 under reduced pressure. All aqueous solutions were prepared from distilled water. β-CD of reagent grade (Shanghai Reagent Factory) was recrystallized twice from water and dried in vacuo at 95 °C for 24 h prior to use. 6-Amino-6-deoxy-β-CD was synthesized according to published procedures.[30]

Instruments

^{1}H, ^{13}C, and 2D NMR spectra were recorded in D_2O on a Bruker AV 400 spectrometer. TGA was performed with a RIGAKU Standard type TG analyzer. Carefully weighed quantities of every sample were subjected at a heating rate of 10.0 K min^{-1} under a nitrogen atmosphere from 25 to 800 °C. FTIR spectra were recorded on a Bio-Rad FTS6000 spectrometer. Mass spectra were recorded on a Varian 7.0T FTICR mass spectrometer (MALDI). All microcalorimetric experiments were performed on a thermostated and fully computer-operated isothermal calorimetry (VP-ITC) instrument (Microcal Inc., Northampton, MA). UV/Vis spectra were recorded in a quartz cell (light path 5 mm) on a Shimadzu UV-3600 spectrophotometer equipped with a PTC-384WI temperature controller. The ICP-AES data were measured by means of an ICP-9000 (N+M) instrument (USA, Thermo Jarrell-Ash Corp.). Elemental analysis (C, H, and N) was performed by using a Vario EL Cube elemental analyzer (Elementar Ltd. Corp., Germany). AFM images were examined by means of a Nanoscope IIIa Multimode 8 AFM (Bruker). TEM images were examined by means of a high-resolution transmission electron microscope (Tecnai G2 F20 microscope, FEI) equipped with a CCD camera (Orius 832, Gatan) operating at an acceleration voltage of 200 kV. The zeta potential of the nanoparticles was recorded by means of a Zeta-Plus ζ potential analyzer (Zetapals/BI-200SM, Brookhaven, USA).

Absorption Spectroscopy

Samples for absorption spectroscopic measurements were prepared by adding an aqueous solution of ct-DNA (Beijing Dingguo Changsheng Biotechnology Co. Ltd.) to an aqueous solution of **2** (or **2**/**3**). The ct-DNA concentration per nucleotide was determined by measuring the UV absorbance at 260 nm ($\varepsilon = 6600\,\text{M}^{-1}\,\text{cm}^{-1}$).[31] The stock solution of ct-DNA was stored at 4 °C and kept at room temperature for 1 h before use.

Fluorescence Measurements

Fluorescence experiments were performed in a conventional quartz cell (light path 10 mm) on a Varian Cary Eclipse equipped with a Varian Cary single-cell Peltier accessory to control the temperature (λ_{ex} = 366.0 nm, bandwidth(ex) = 2.5 nm, bandwidth(em) = 10.0 nm) at 25 °C in 5 mM Tris-HCl 50 mM NaCl buffer (pH 7.1).

AFM Measurements

Samples were prepared by dropping the solution on mica. The mica samples were then air-dried and the samples were examined in tapping mode.

TEM Measurements

Each sample for TEM measurements was prepared by dropping sample solution (50 μL) on a copper grid. The grids were then air-dried and the samples were examined by means of a high-resolution TEM instrument.

Cell Culture

The human breast cancer MCF-7 cell line was cultured in Dulbecco's modified eagle medium (DMEM) supplemented with 10% fetal bovine serum (FBS) at 37 °C in a humidified atmosphere of 5% of CO_2.

Agarose Gel Electrophoresis

Agarose gels of 1% were prepared by heating agarose (250 mg) in TAE buffer (25 mL; 4.0×10^{-2} mol L^{-1} Tris, 2.0×10^{-2} mol L^{-1} acetic acid, 2×10^{-3} mol L^{-1} ethylenediaminetetraacetic acid (EDTA); Dingguo Changsheng Biotechnology Co. Ltd.). Sample solutions containing pBR322 DNA, **2**, and **3** with different w/w/w ratios were prepared by adding an appropriate volume of solutions of **2**, **3**, and DNA into Eppendorf tubes, which were then diluted to a total volume of 10 μL. After incubation at 4 °C for 30 min, the sample solutions were subjected to electrophoresis at 60 V for 1 h (current 120 mA) and visualized by ethidium bromide staining. The DNA bands were visualized and photographed by means of a UV transilluminator and WD-9413B gel documentation system (Beijing Liuyi Instrument Factory, P.R. China).

Cytotoxicity Studies

The cytotoxicity of **2**/**3** was investigated by means of a 3-(4,5-dimethylthiazol-2-yl)-2,5-diphenyltetrazolium bromide (MTT; Sigma, St. Louis, MO, USA) viability test on the MCF-7 cell line. Briefly, cells were plated at a density of 1.0×10^4 cells per well in 96 wells. After 24 h of incubation, cells were treated with **2**/**3** at indicated concentrations for 48 h, then the medium was removed, and fresh medium (200 μL) plus MTT reagent (20 μL; 2.5 mg dissolved in 50 μL of dimethylsulfoxide (DMSO)) were added to each well. After incubation for 4 h at 37 °C, the culture medium containing MTT was withdrawn and DMSO (200 μL) was added, followed by shaking for 10 min until the crystals dissolved. Viable cells were detected by measuring the absorbance at $\lambda = 490$ nm by using an MRX II absorbance reader (DYNEX Technologies, Chantilly, VA, USA). Cell growth was expressed as a percentage of absorbance in cells treated with **2**/**3** to that in cells without **2**/**3** treatment (100%). The survival rate (IR) was calculated as follows: IR = (A value of **2**/**3** well/A value of control well) × 100%.

*Synthesis of **1***

DL-Lipoic acid (227.0 mg, 1.1 mmol), *O*-(7-azabenzotriazol-1-yl)-*N*,*N*,*N*′,*N*′-tetramethyluronium hexafluorophosphate (HATU; 418.3 mg, 1.1 mmol), hydroxybenzotriazole (HOBt; 675.2 mg, 5.0 mmol), and 4-dimethylaminopyridine (DMAP; 61.09 mg, 0.5 mmol) were dissolved in DMF (10 mL) at 0 °C. The mixture was stirred for 1 h at 0 °C under an argon atmosphere, and then a solution of DMF (10 mL) containing 6-amino-6-deoxy-β-CD (1.1 g, 1.0 mmol) was added. The reaction mixture was stirred for 6 h at 0 °C and then for 8 h at room temperature under an argon atmosphere. The mixture was poured into acetone (300 mL). The precipitate was collected by filtration to obtain a yellow powder, which was purified by column chromatography on silica gel by using propanol/water/ammonia (v/v/v 6:3:1) as the eluent to obtain **1** as a white solid (501.2 mg, 37.9%). ^{1}H NMR ([D$_6$]DMSO, 400 MHz): δ = 1.22–1.38 (m, 2H), 1.42–1.68 (m, 4H), 1.82–1.93 (m, 1H), 2.05–2.17 (m, 2H), 2.32–2.45, (m, 1H), 3.06–3.19 (m, 3H), 3.26–3.32 (m, 14H), 3.53–3.75 (m, 28H), 4.37–4.61 (m, 6H), 4.77–4.90 (m, 7H), 5.59–5.86 (m, 14H), 7.55–7.69 ppm (s, 1H); HRMS (MALDAI): *m*/*z* calcd for $C_{50}H_{83}NO_{35}S_2$ $[M+H]^+$: 1322.4265; found: 1322.4220; elemental analysis calcd (%) for $C_{50}H_{83}NO_{35}S_2\cdot7H_2O$: C 41.46, H 6.75, N 0.97; found: C 41.66, H 7.02, N 0.92.

*Synthesis of **2***

A solution of DMSO (20 mL) containing gold chloride tetrahydrate (50.0 mg, 0.1 mmol) was quickly mixed with another solution of DMSO (20 mL) containing **1** (20.0 mg, 0.02 mmol) and sodium borohydride (75.5 mg, 2.0 mmol). The reaction mixture was stirred for 24 h at room temperature, and then acetonitrile (40 mL) was added. The precipitate was collected by centrifugation and washed with DMSO/CH_3CN (100 mL; v/v 1:1) and ethanol (100 mL). Subsequently, the product was purified by dialysis (molecular weight cutoff 3500) in distilled water sev-

eral times and dried under vacuum for 12 h at 80 °C. From the elemental analysis and ICP-AES data, the content of CD units (W_{CD}) was calculated to be 0.162 mmol g^{-1}; the average number of β-CD units around one nanoparticle was calculated to be 14. Elemental analysis (%) found: C 9.73, H 2.73, N 0.30; ICP-AES (%): Au 25.7.

Synthesis of ***3***

9-Anthracene carboxaldehyde (1.1 g, 5.0 mmol) and diethylenetriamine (2.7 mL, 25 mmol) were dissolved in a mixture of anhydrous ethanol (125 mL) and dichloromethane (75 mL), and stirred for 24 h at room temperature. Sodium borohydride (1.9 g, 50 mmol) was then added and the reaction mixture was stirred for 8 h at room temperature. The solvent was removed at reduced pressure. The resulting residue was washed with water (50 mL) and extracted with dichloromethane (200 mL) three times. The organic phase was collected and dried with anhydrous sodium sulfate, and the solvent was removed under low pressure to give the crude N-(2-aminoethyl)-N'-(9-anthracenylmethyl)-1,2-ethanediamine, which was dried under vacuum and used without further purification. Adamantane-1-carboxylic acid (0.9 g, 5.0 mmol) was stirred for 4 h in distilled thionyl chloride (5 mL) at 70 °C under an argon atmosphere. Excess thionyl chloride was evaporated to give the free acyl chloride (0.9 g, 90.5%). Adamantane-1-carbonyl chloride[32] was dissolved in dichloromethane (20 mL) and added dropwise to a solution of triethylamine (2.1 mL, 15 mmol) and *N*-(2-aminoethyl)-*N'*-(9-anthracenylmethyl)-1,2-ethanediamine[33] (1.5 g, 5 mmol) in anhydrous dichloromethane (20 mL) at room temperature under an argon atmosphere. The reaction mixture was stirred for 8 h at room temperature under an argon atmosphere. The solvent was evaporated under vacuum and the residue was purified by column chromatography on silica gel by using dichloromethane/methanol (v/v 10:1) as the eluent to give **3** as a white powder (1.27 g, 55.7%). ^{1}H NMR (D_2O, 400 MHz): δ = 1.47–1.72 (m, 12H), 1.84–1.93 (s, 3H), 3.00–3.09 (t, 2H), 3.27–3.50 (m, 6H), 5.08–5.15 (s, 2H), 7.53–7.61 (t, 2H), 7.63–7.72 (t, 2H), 8.04–8.13 (d, 2H), 8.18–8.26 (d, 2H), 8.56–8.62 ppm (s, 1H); ^{13}C NMR (D_2O, 400 MHz): δ = 183.1, 130.9, 130.2, 129.5, 127.7, 125.5, 122.7, 47.7, 43.5, 40.4, 38.2, 36.2, 35.6, 27.5 ppm; HRMS (MALDAI): *m/z* calcd for $C_{30}H_{37}N_3O$ $[M+H]^+$: 456.3015; found: 456.3013; elemental analysis calcd (%) for $C_{30}H_{37}N_3O{\cdot}5H_2O$: C 66.03, H 8.68, N 7.70; found: C 66.29, H 8.64, N 8.00.

Acknowledgements

We thank the 973 Program (2011CB932502) and the NNSFC (91227107 and 21272125) for financial support.

[1] C. Sheridan, *Nat. Biotechnol.* **2011**, *29*, 121–128.
[2] R. Niven, R. Pearlman, T. Wedeking, J. Mackeigan, P. Noker, L. Simpson-Herren, J. G. Smith, *J. Pharm. Sci.* **1998**, *87*, 1292–1299.
[3] C. Ortiz Mellet, J. M. García Fernández, J. M. Benito, *Chem. Soc. Rev.* **2011**, *40*, 1586–1608.
[4] T. Tanaka, Y. Cao, J. Folkman, H. A. Fine, *Cancer Res.* **1998**, *58*, 3362–3369.
[5] P. L. Felgner, T. R. Gadek, M. Holm, R. Roman, H. W. Chan, M. Wenz, J. P. Northrop, G. M. Ringold, M. Danielsen, *Proc. Natl. Acad. Sci. USA* **1987**, *84*, 7413–7417.
[6] T. Ooya, H. S. Choi, A. Yamashita, N. Yui, Y. Sugaya, A. Kano, A. Maruyama, H. Akita, R. Ito, K. Kogure, H. Harashima, *J. Am. Chem. Soc.* **2006**, *128*, 3852–3853.
[7] J. Haensler, F. C. Szoka, Jr., *Bioconjug. Chem.* **1993**, *4*, 372–379.
[8] H. Wang, Y. Chen, X.-Y. Li, Y. Liu, *Mol. Pharm.* **2007**, *4*, 189–198.
[9] E. E. Connor, J. Mwamuka, A. Gole, C. J. Murphy, M. D. Wyatt, *Small* **2005**, *1*, 325–327.
[10] a) D. Shenoy, S. Little, R. Langer, M. Amiji, *Mol. Pharm.* **2005**, *2*, 357–366; b) S. K. Sahoo, V. Labhasetwar, *Mol. Pharm.* **2005**, *2*, 373–383.
[11] G. Han, C. T. Martin, V. M. Rotello, *Chem. Biol. Drug Des.* **2006**, *67*, 78–82.
[12] G. Han, C.-C. You, B.-J. Kim, R. S. Turingan, N. S. Forbes, C. T. Martin, V. M. Rotello, *Angew. Chem. Int. Ed.* **2006**, *45*, 3165–3169; *Angew. Chem.* **2006**, *118*, 3237–3241.
[13] M. Thomas, A. M. Klibanov, *Proc. Natl. Acad. Sci. USA* **2003**, *100*, 9138–9143.
[14] a) Y. Liu, C.-F. Ke, H.-Y. Zhang, W.-J. Wu, J. Shi, *J. Org. Chem.* **2007**, *72*, 280–283; b) S. Angelos, N. M. Khashab, Y.-W. Yang, A. Trabolsi, H. A. Khatib, J. F. Stoddart, J. I. Zink, *J. Am. Chem. Soc.* **2009**, *131*, 12912–12914; c) C. Kim, S. S. Agasti, Z. Zhu, L. Isaacs, V. M. Rotello, *Nat. Chem.* **2010**, *2*, 962–966.
[15] R. Zidovetzki, I. Levitan, *Biochim. Biophys. Acta Biomembr.* **2007**, *1768*, 1311–1324.
[16] I. Habus, Q. Zhao, S. Agrawal, *Bioconjugate Chem.* **1995**, *6*, 327–331.
[17] a) Q. Zhao, J. Temsamani, P. L. Iadarola, S. Agrawal, *Biochem. Pharmacol.* **1996**, *52*, 1537–1544; b) Q. Zhao, J. Temsamani, S. Agrawal, US Patent US6667293 B1.
[18] a) Y. Liu, L. Yu, Y. Chen, Y.-L. Zhao, H. Yang, *J. Am. Chem. Soc.* **2007**, *129*, 10656–10657; b) Y. Liu, Z.-L. Yu, Y.-M. Zhang, D.-S. Guo, Y.-P. Liu, *J. Am. Chem. Soc.* **2008**, *130*, 10431–10439; c) Y. Chen, L. Yu, X.-Z. Feng, S. Hou, Y. Liu, *Chem. Commun.* **2009**, 4106–4108.
[19] B. D. Chithrani, A. A. Ghazani, W. C. W. Chan, *Nano Lett.* **2006**, *6*, 662–668.
[20] M. V. Rekharsky, Y. Inoue, *Chem. Rev.* **1998**, *98*, 1875–1918.
[21] a) A. A. Bothner-By, R. L. Stephens, J. Lee, C. D. Warren, R. W. Jeanloz, *J. Am. Chem. Soc.* **1984**, *106*, 811–813; b) D. Neuhaus, M. Williamson in *The Nuclear Overhauser Effect in Structural and Conformational Analysis*, 2nd ed., Wiley-VCH, New York, **1989**, p. 123.
[22] C. V. Kumar, E. H. Asuncion, *J. Am. Chem. Soc.* **1993**, *115*, 8547–8553.
[23] J. J. Storhoff, A. A. Lazarides, R. C. Mucic, C. A. Mirkin, R. L. Letsinger, G. C. Schatz, *J. Am. Chem. Soc.* **2000**, *122*, 4640–4650.
[24] M. Mandelkern, J. G. Elias, D. Eden, D. M. Crothers, *J. Mol. Biol.* **1981**, *152*, 153–161.
[25] L. A. Dykman, N. G. Khlebtsov, *Chem. Rev.* **2014**, *114*, 1258–1288.
[26] a) J. Rejman, V. Oberle, I. S. Zuhorn, D. Hoekstra, *Biochem. J.* **2004**, *377*, 159–169; b) W. Zauner, N. A. Farrow, A. M. Haines, *J. Controlled Release* **2001**, *71*, 39–51; c) H. Hillaireau, P. Couvreur, *Cell. Mol. Life Sci.* **2009**, *66*, 2873–2896.
[27] Y. Liu, Y. Chen, Z.-Y. Duan, X.-Z. Feng, S. Hou, C. Wang, R. Wang, *ACS Nano* **2007**, *1*, 313–318.
[28] D. Lochmann, E. Jauk, A. Zimmer, *Eur. J. Pharm. Biopharm.* **2004**, *58*, 237–251.
[29] M.-L. Ainalem, T. Nylander, *Soft Matter* **2011**, *7*, 4577–4594.
[30] S. Brown, J. Coates, D. Coghlan, C. Easton, S. Vaneyk, W. Janowski, A. Lepore, S. Lincoln, Y. Luo, B. May, D. Schiesser, P. Wang, M. Williams, *Aust. J. Chem.* **1993**, *46*, 953–958.
[31] M. F. Ottaviani, F. Furini, A. Casini, N. J. Turro, S. Jockusch, D. A. Tomalia, L. Messori, *Micromolecules* **2000**, *33*, 7842–7851.
[32] L. F. Fieser, M. Z. Nazer, *J. Med. Chem.* **1967**, *10*, 517–521.
[33] L. Rodríguez, S. Alves, J. C. Lima, A. J. Parola, F. Pina, C. Soriano, T. Albelda, E. García-España, *J. Photochem. Photobiol. A* **2003**, *159*, 253–258.

Received: February 18, 2014
Published online: May 26, 2014